Rotating Detonation Rocket Engine Operation in 10-mm and 25-mm Coreless Combustors

Carl Knowlen, Tyler Mundt, Quentin Roberts, and Mitsuru Kurosaka
William E. Boeing Department of Aeronautics and Astronautics, University of Washington
Seattle, WA 98195, USA

1 Introduction

The feasibility of operating small scale rotating detonation rocket engines with annular combustors having diameters from 28-mm to as small as 10-mm has been demonstrated [1-4]. When operating with propellant mass fluxes needed for the thrust range 20 N to 200 N, however, the intense heat transfer to the inner core limits continuous operation to only a few seconds before significant erosion is experienced [3], even when using high temperature resistant materials such as molybdenum [4]. Although composite ceramics and/or other refractory materials may eventually be developed that enable heat-soaked operation of small-scale RDREs, there is immediate interest in operating cylindrical combustors to exploit the advantages of detonation combustion propulsive cycles. Coreless RDRE operation has been demonstrated by various facilities with combustor diameters of 25-mm and less [2-5]. In general, the coreless RDRE performance reported in these investigations was somewhat lower than with that of annular combustors; nonetheless, their efficacy has been well established. In order to contribute to this growing technical database, the results of an experimental investigation of coreless RDRE operation in 10-mm and 25-mm combustors with CH_4-O_2 and H_2-O_2 propellants were presented here.

2 Experimental Facility

The Rotating Detonation Engine test facility is located in an interior laboratory space that has a 4 m^3 dump tank rated from vacuum to 0.7 MPa working pressure for capturing and condensing combustion effluent. The 0.25-m-diameter wye tube shown in Fig. 1 connects the dump tank to the RDRE rigs on the test stand. Through an observation port, the wave dynamics within the RDRE combustors were observed at frame rates up to 450,000 FPS at 1 µs exposure with Phantom digital video cameras using either a 70-200 mm or 200-500 mm zoom lens.

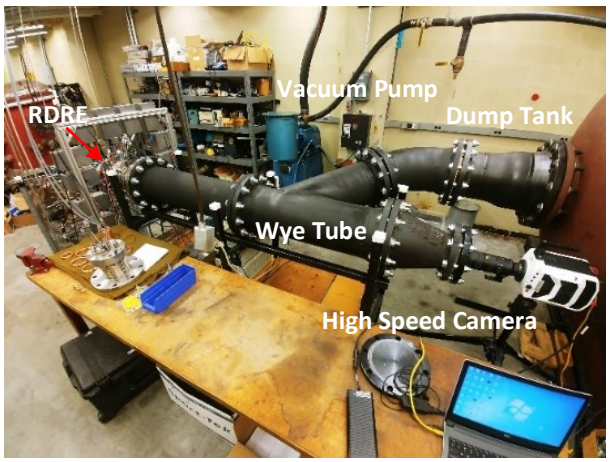

Figure 1: High enthalpy test facility wye tube routes combustion effluent to dump tank.

Correspondence to: knowlen@aa.washington.edu

Oxidizer and fuel flows were controlled with electronic regulators (TESCOM ER5000 and TESCOM 44-4000 series regulators). Flow measurements were made with precision pressure transducers and low noise thermal couples in approach tubes that were factory calibrated with critical flow nozzles (CFNs). Combinations of various Fluid-Dyne CFNs, fabricated from Monel® for oxidizer compatibility, enabled experiments with propellant mass flow rates ranging from 0.006 kg/s to 0.44 kg/s and equivalence ratio range of $0.2 < \phi < 2.8$ with a net uncertainty in mass flow rate and equivalence ratio of ±1.5% [3,4].

3 RDRE Geometry

The coreless RDREs utilized the same endcap (SS304) with different injectors (brass) and outer wall (OFHC copper) geometries as shown in Fig. 2. The 10-mm- and 25-mm-combustors were 20-mm-long and 25-mm-long, respectively. The injectors were sandwiched between the outer core and endcap, which had alignment features to center the injectors to within 0.026 mm of the centerline of the cylindrical combustors. Combustion products flowed through the 10-mm and 25-mm-combustor exits into 25-mm-long cylindrical sections having either 51-mm- or 76-mm-diameters, respectively.

The oxidizer (oxygen) gas flowed through four feedlines into an outer annular plenum within the endcap, which in turn fed a thinner annular disk with drilled injector ports. The plenum pressure and temperature for the oxidizer injectors were measured in the outer annulus. For 10-mm-combustor, the fuel (methane or hydrogen) flowed through a 25-mm welded fitting to an eight-port distributor (3.2-mm-diameter holes) with a threaded center hole to a 25-mm-O.D. disk volume. The flow then entered a 4.8-mm-diameter blind hole with fuel injector ports drilled into its base. (Fig. 2-left). In the 25-mm-combustor, the threaded center hole was used to retain the injector and only the outer eight ports fed the coaxial annular fuel plenum (Fig. 2-right). Fuel plenum pressure and temperature were measured in a plumbing tee (not shown) connected to the 25-mm weld-port fitting at the rear of the test rig. Based on the area profiles of the plenum passageways, their pressure drops were negligible relative to those of the injector ports at the fuel mass flow rates considered in this investigation.

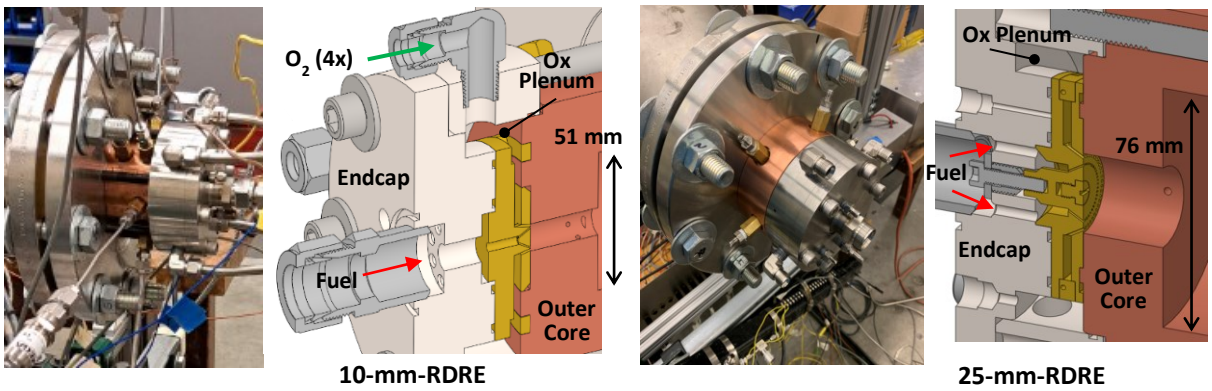

Figure 2: RDRE configurations. Left: 10-mm-combustor. Right: 25-mm-combustor.

Pressure transducers (OMEGA PX319-500A5V) with snubbers were mounted at the end of stand-off tubes having an internal passage length-to-diameter ratio of 145 in the sidewall and plena of both combustors. Also installed in the plena were exposed-bead Type K thermocouples (OMEGA TJ36-CASS-116E-12). These sensors were sampled at 2 kHz via a National Instruments-based 32-channel data acquisition system. For detonation initiation, a spark-ignited pre-detonator using methane-oxygen reactants was mounted into the last port of the combustor annulus. The pre-detonator was fired tangentially in the 10-mm-combustor and radially inward in the 25-mm-combustor 200 ms to 300 ms after the fuel and oxidizer flows were switched on. The combustion process exhibited transient wave behavior that typically established one of several potential steady state operating modes within the first 200 ms after firing the pre-detonator. Data from the last 100 ms of the run were averaged for each test.

Listed in Tables 1 and 2 are the distances relative to the injector faces and azimuthal orientations clocked from vertical of all instrument ports in the 10-mm- and 25-mm-combustors, respectively. There were five sidewall ports spaced 2 mm apart in the 10-mm-combustor for measuring the axial pressure gradient (Table 1). At the first axial station there were also two larger ports with angular spacing of 120˚ for the piezoelectric transducers (PCB 113 sampled at 1.25 MHz) that enabled wave frequency and spin direction to be determined. At the mid-point of the combustor (10 mm), a thermocouple well port (1.65-mm-dia.) was drilled to within 6 mm of the combustion chamber outer wall to monitor wall temperature transients during operation. An additional port near the combustor exit oriented tangentially to outer diameter of the chamber was used for the pre-detonator ignitor. There was also a pressure port downstream of the combustor in the 51-mm-diameter section for back pressure measurements. The 25-mm-combustor had four sidewall pressure ports spaced approximately 2 mm apart that spiraled around the periphery to allow sufficient room for the adaptor plugs and installation tools as indicated in Table 2. The pre-detonator port was opposite the last instrument port in the combustor and downstream of the combustor exit in the adjacent 76-mm-dia section was a pressure port for back pressure measurements.

Table 1 Instrument port locations for 10-mm-Combustor

Parameter	Combustor: 10-mm-OD x 20-mm-long								Exit	51-mm-OD	Pre-Det
x, mm	9.0	9.0	9.0	10.0	11.0	13.0	15.0	17.0	20.0	33.0	17.0
Dia, mm	1.57	2.29	2.29	TC	1.57	1.57	1.57	1.57	-	1.57	2.38
Angle, deg	345	180	300	60	165	105	195	45	-	345	225

Table 2 Instrument port locations for 25-mm-Combustor

Parameter	Combustor: 25.4-mm-OD x 25.4-mm-long				Exit	76-mm-OD	Pre-Det
x, mm	16.5	18.5	20.3	22.4	25.4	38.1	22.4
Dia, mm	2.38	2.38	2.38	2.38	-	2.38	3.18
Angle, deg	0	60	240	120	-	180	180

Images and section views of the flat-faced, impinging injectors were shown in Fig. 3. Their design details can be found in [3, 4]. Port diameters (d_o = 0.81 mm and d_f = 0.51 mm) and area ratios (A_o/A_f = 2.56) were the same for these two injectors, resulting in the fuel and oxidizer plena having the same injector pressure drop at a fuel equivalence ratio of 1.08 with CH_4-O_2 and 0.78 for H_2-O_2. The injector-to-combustor area ratios, however, differed from 0.11 for the 10-mm-RDRE to 0.067 for 25-mm-RDRE, resulting in the larger combustor having stiffer injectors at a given propellant mass flux. The 10-mm-RDRE had 12 pairs of injectors with the oxidizer ports angled inward at 11.3º toward the combustor centerline and the fuel ports angled outward at 30º with impingement diameter of 8.5 mm. Their impingement angle resulted in axial flow at equivalence ratios of 1.15 for CH_4-O_2 and 0.78 for H_2-O_2. The 25-mm-RDRE had 48 pairs of injectors with the oxidizer ports angled inward at 30º toward the combustor centerline and the fuel ports angled outward at 30º with impingement diameter of 20.4 mm. Their impingement angle was such that the injectant flows were radially momentum balanced at equivalence ratios of 2.93 for CH_4-O_2 and 1.99 for H_2-O_2.

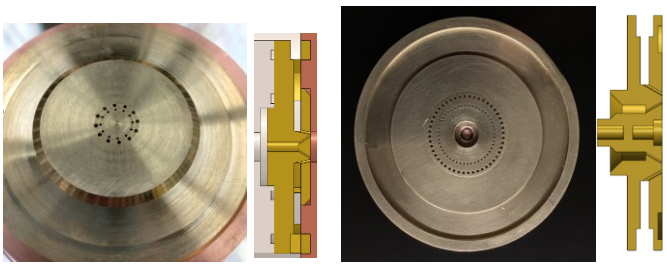

Figure 3: Injector designs. Left: 10-mm-combustor. Right: 25-mm-combustor.

4 Experimental Results

Equivalence ratio, ϕ, sweeps with two coreless RDRE combustors were carried out at various propellant mass fluxes, $\dot{m}_f$, and in all cases the back pressure was 50 kPa. Mass flux sweeps with both CH_4-O_2 and H_2-O_2 were carried out at constant equivalence ratio of $\phi \sim 1.15$. Sweeps of equivalence ratio over $0.4 < \phi < 1.8$ and $0.25 < \phi < 2.6$ in the 10-mm- and 25-mm-combustors, respectively, were carried out at $\dot{m}_f \sim 160$ kg/s/m^2 and $\dot{m}_f \sim 240$ kg/s/m^2. Most data represent the average of at least two experiments that were within 2% of desired test conditions. In these coreless combustors, wave dynamics consisted of single spinning waves, two or three co-rotating waves, axial pulsing, or deflagration as indicated by the plotting symbols in Fig. 4. No counter-rotating wave systems were observed in these experiments.

Spinning wave operation was established at all conditions tested with H_2-O_2 in the 10-mm-combustor (Fig. 4a) with wave numbers of either 1, 2, or 3. Single wave operation occurred throughout the equivalence ratio range tested with $\dot{m}_f < 190$ kg/s/m^2, except for a few cases near stoichiometric in which two waves appeared. Regions where operation with two different wave systems were possible typically indicated conditions at which mode transitions occur. Indeed, the wave count became two for near stoichiometric flow while 200 kg/s/m^2 $< \dot{m}_f <$ 280 kg/s/m^2 and three when $\dot{m}_f > 285$ kg/s/m^2.

Deflagration inside the 10-mm-combustor in fuel lean tests always occurred when using CH_4-O_2 propellant, as indicated in Fig. 4b. Over the range of mass flux tested here (100 kg/s/m^2 $< \dot{m}_f <$ 320 kg/s/m^2), a relatively sharp boundary between deflagration and one wave operation was found at $\phi \sim 1.15$. Stable one wave operation was observed in the fuel rich region up to $\phi \sim 1.8$. Note, deflagration occurred in the stoichiometric region even at the highest mass flux tested.

The operation mode at constant $\phi = 1.15$ for the 25-mm-combustor, shown in Fig. 4c, underwent a transition from deflagration to one spinning wave between 160 kg/s/m^2 $< \dot{m}_f <$ 240 kg/s/m^2. At the highest mass flux tested (505 kg/s/m^2), however, only a single spinning wave was observed, which indicated that even higher fluxes were required to establish a co-rotating two-wave system in this combustor. At a mass flux of 240 kg/s/m^2, one spinning wave was present when $\phi > 0.3$ with deflagration otherwise occurring. At the mass flux of 160 kg/s/m^2, however, one wave operation was only established within $0.3 < \phi < 0.7$, with deflagration at all other equivalence ratios except $\phi \sim 2.0$, where steady axial pulsations were observed.

Wave spin speed, D_{spin}, data in the 10-mm-combustor from ϕ sweeps with H_2-O_2 propellant at various mass flux ratios were plotted in Fig. 5a with Chapman-Jouguet detonation speed (D_{CJ}) (based on STP initial conditions) and the corresponding spin frequency for each wave system. For one wave operation, average D_{spin} was 2.93 km/s over the

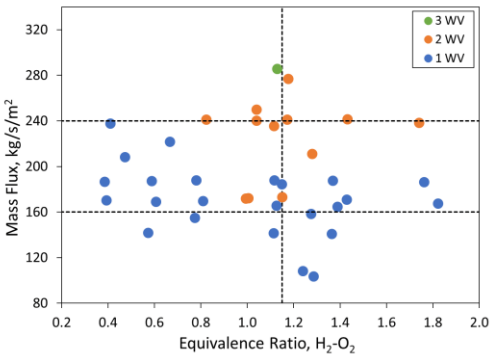

(a) 10-mm-combustor

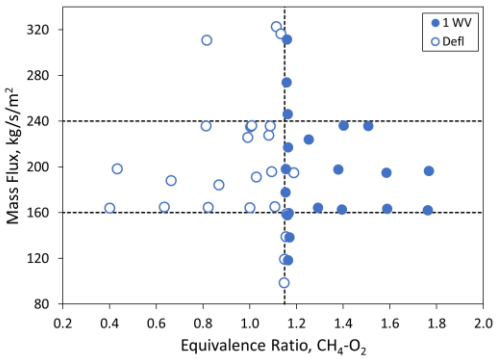

(b) 10-mm-combustor

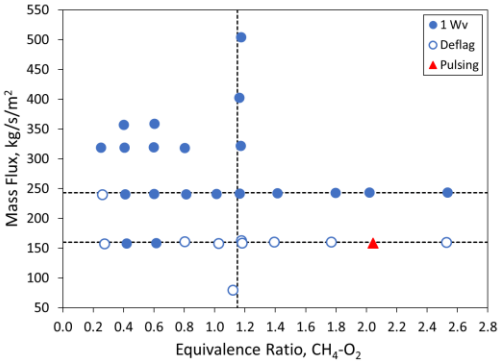

(c) 25-mm-combustor

Figure 4: Wave dynamic results for coreless combustor test matrix. Propellants: (a) H_2-O_2 (b) CH_4-O_2 (c) CH_4-O_2

range of ϕ explored, which was greater than D_{CJ} under fuel lean conditions. At higher mass flux conditions where there were two waves, the average D_{spin} value was ~2.10 km/s with a standard deviation of ~2.5%. The maximum observed operating frequency (167 kHz) occurred in the three wave system.

Wave spin speed and corresponding spin frequency versus equivalence ratio data plotted in Fig. 5b were from ϕ sweeps with CH_4-O_2 propellant at the mass fluxes indicated in the legend. In the 10-mm-combustor, there was only one spinning wave during RDRE operation for all tests with CH_4-O_2. The D_{spin} data varied from 1.99 km/s to 2.07 km/s (corresponding to spin frequencies of ~63 kHz to ~66 kHz) in the fuel rich conditions of these ϕ sweeps. Polynomial trend lines indicated D_{spin} maxima were in the equivalence ratio range of $1.4 < \phi < 1.5$.

Wave spin-to-CJ speed ratio, D_{spin}/D_{CJ}, data for the 25-mm-combustor at $\dot{m}_f = 240$ kg/s/m^2 and D_{CJ} for CH_4-O_2 propellant were plotted in Fig. 5c. As ϕ decreased, the spin speed increased until $\phi \sim 0.4$, where it reached ~2.3 km/s. Note that $D_{spin} > D_{CJ}$ when $\phi < 0.5$, which was a similar finding for one wave operation in the 10-mm-combustor when $\phi < 1.0$ in H_2-O_2. If injector impingement diameters were used instead of combustor diameters for determining D_{spin}, then max D_{spin}/D_{CJ} for the 25-mm and 10-mm combustors would be ~0.93 and ~1.11, respectively, which implies that the 10-mm combustor maximum reference diameter should be 7.7 mm if D_{CJ} was indeed the actual the spin speed limit.

Axial pressure profiles for $\phi \sim 1.15$ tests were plotted in Fig. 6 with wave numbers indicated and legends having corresponding mass fluxes (kg/s/m^2). The 10-mm-experiments with H_2-O_2 at $\dot{m}_f \sim 285$ kg/s/m^2 in Fig. 6a had three co-rotating waves. In this case, the peak pressure (~450 kPa) at the station 9 mm from the injector face decreased by more than 100 kPa by the 17 mm station that was 3 mm from the exit. Lower mass flux tests resulted in lower pressure, regardless of the wave number.

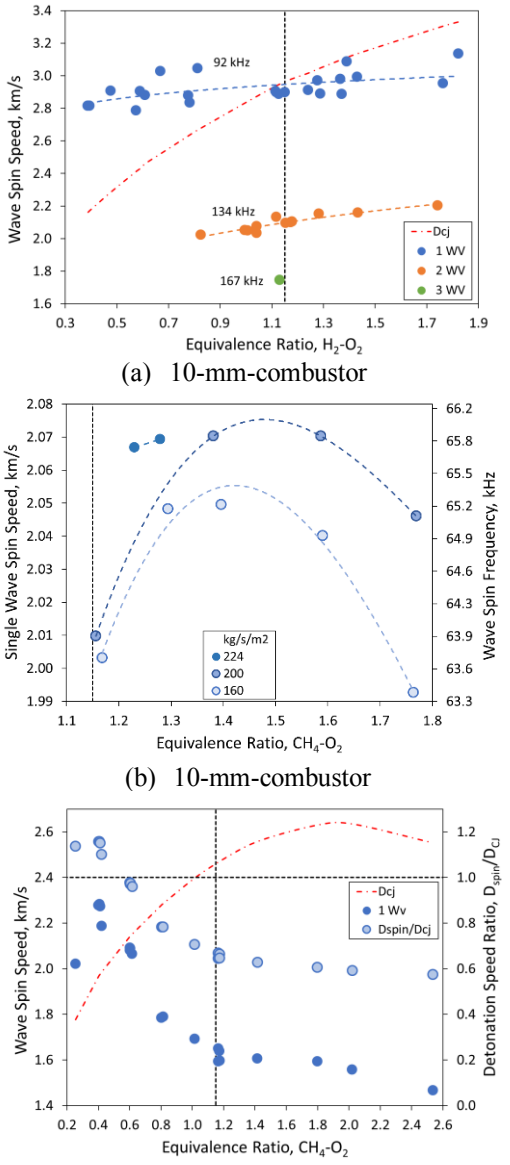

(a) 10-mm-combustor

(b) 10-mm-combustor

(c) 25-mm-combustor

Figure 5: Wave spin speeds, spin frequencies, and CJ speed ratio for coreless combustors. Propellants: (a) H_2-O_2 (b) CH_4-O_2 (c) CH_4-O_2

When fueled with CH_4-O_2 propellant at the same mass flux as H_2-O_2, the 10-mm-combustor pressure measurements at the 9 mm station were within ~5%. The pressure gradients with CH_4-O_2, however, were ~50% steeper. Below a mass flux of ~100 kg/s/m^2, deflagration resulted in much lower pressure at the 9 mm station that increased axially in a manner consistent with weak supersonic combustion.

The first pressure port in the 25-mm-combustor was 16.5 mm from the injector face. At the same equivalence ratio and mass flux of CH_4-O_2, the pressures in the larger combustor were ~10% lower. This discrepancy may be due to the first station being ~7 mm farther downstream and thus not as close to the detonation zone. Nonetheless, the amplitudes and trends of the axial pressure profiles were in good agreement between the 10-mm and 25-mm-combustors. Even the deflagration pressure gradients were comparable.

5 Discussion and Summary

The RDRE wave dynamics in the 10-mm and 25-mm coreless combustors with CH_4-O_2 propellant were similar in that they both operated with only one spinning wave and no counter-rotating waves. A major difference, however, was that the 10-mm-combustor would not operate with a spinning wave under fuel lean conditions in CH_4-O_2. Conversely, single spinning waves at fuel-lean and fuel-rich conditions were readily established with H_2-O_2 propellant in the 10-mm-combustor with co-rotating multiple wave systems occurring when mass flux increased beyond 200 kg/s/m^2.

Wave spin speeds were typically 60% to 80% CJ speed in fuel rich propellants. Under fuel lean conditions, however, wave spin speeds were close to CJ speed when based on the impingement diameters of the injectors. In all cases, the axial pressures were proportional to mass flux with corresponding peak amplitudes being within 10% regardless of combustor diameter or propellant composition.

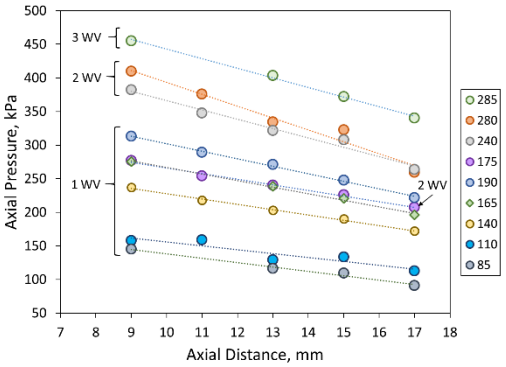

(a) 10-mm-combustor with H_2-O_2

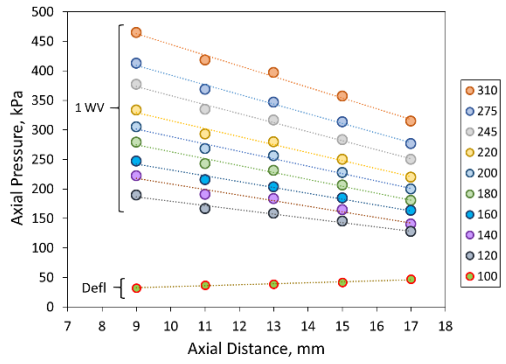

(b) 10-mm-combustor with CH_4-O_2

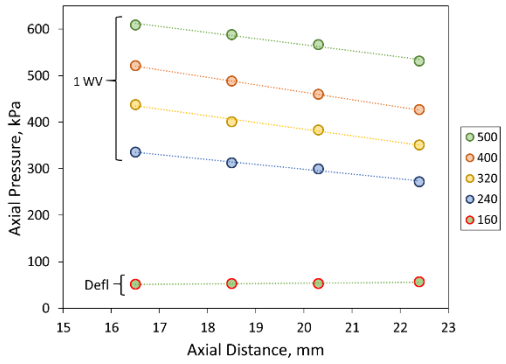

(c) 25-mm-combustor with CH_4-O_2

Figure 6: Axial pressure for $\phi = 1.15$ plotted from coreless combustors with mass flux (kg/s/m^2) in legends. Propellants: (a) H_2-O_2 (b) CH_4-O_2 (c) CH_4-O_2

Acknowledgments

This work was supported by AFOSR Grant FA 9550-18-1-9-0076 with program manager Dr. Chiping Li and Jacobs Technology contract FA 9300-20-F-9801 with program manager Dr. Eric Paulson. UW STF program provided the Phantom cameras used on this project.

References

[1] Fiorino NT, Snow NJ, Schauer FR, Polanka MD, Schumaker S, Sell B. (2023) Improving Detonability in a Small-Scale Rotating Detonation Engine Using Partial Premixing. J Prop & Power. 39, 232.

[2] Durkee KJ, Dave RT, Maybee MA, Cobb GR, Burr JR, Bennewitz JW. (2025) Performance Comparison of Variable Center Body Configurations for a 25 mm Rotating Detonation Rocket Engine. doi: 10.2514/6.2025-0995.

[3] Mundt T, Chang L, Ikeda M, Menn D, Knowlen C, Kurosaka M. (2023) Annular Gap Width Variation in 25-mm Rotating Detonation Rocket Engine. doi: 10.2514/6.2023-1103.

[4] Knowlen C, Mundt T, Roberts Q, Hamza A, Menn D, Kurosaka M. (2024) Operating Characteristics of a 10-mm Rotating Detonation Rocket Engine. doi: 10.2514/6.2024-2610.

[5] Goto K, Ota K, Kawasaki A, Itouyama N, Watanabe H, Matsuoka K, Kasahara J, Matsuo A, Funaki I, Kawashima H. (2022) Cylindrical Rotating Detonation Engine with Propellant Injection Cooling. J Prop & Power. 38, 410.